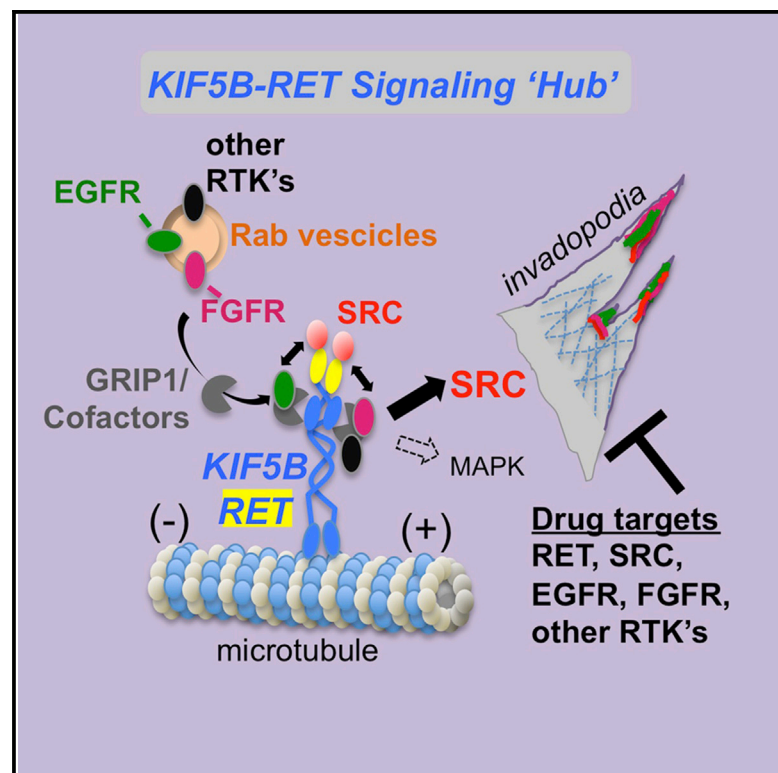


KIF5B-RET Oncoprotein Signals through a Multi-kinase Signaling Hub

Graphical Abstract



Authors

Tirtha Kamal Das, Ross Leigh Cagan

Correspondence

tirtha.das@mssm.edu

In Brief

Das and Cagan find that each portion of the KIF5B-RET fusion oncoprotein recruits different components to assemble a multi-kinase oncogenic signaling hub that promotes invadopodia formation. This suggests that multiple kinase components of this KIF5B-RET hub need to be simultaneously targeted therapeutically.

Highlights

- The KIF5B-RET kinesin domain activates various RTKs via RAB vesicles
- The RET kinase domain activates canonical pathways, including SRC
- This multi-kinase hub shows enhanced signaling activity and promotes invadopodia
- Optimal drugs against KIF5B-RET should target RET, EGFR, FGFR, PDGFR, and SRC



KIF5B-RET Oncoprotein Signals through a Multi-kinase Signaling Hub

Tirtha Kamal Das^{1,2,*} and Ross Leigh Cagan¹

¹Department of Cell, Developmental and Regenerative Biology and School of Biomedical Sciences, Icahn School of Medicine at Mount Sinai, One Gustave Levy Place, New York, NY 10029-1020, USA

²Lead Contact

*Correspondence: tirtha.das@mssm.edu

<http://dx.doi.org/10.1016/j.celrep.2017.08.037>

SUMMARY

Gene fusions are increasingly recognized as important cancer drivers. The KIF5B-RET gene has been identified as a primary driver in a subset of lung adenocarcinomas. Targeting human KIF5B-RET to epithelia in *Drosophila* directed multiple aspects of transformation, including hyperproliferation, epithelial-to-mesenchymal transition, invasion, and extension of striking invadopodia-like processes. The KIF5B-RET-transformed human bronchial cell line showed similar aspects of transformation, including invadopodia-like processes. Through a combination of genetic and biochemical studies, we demonstrate that the kinesin and kinase domains of KIF5B-RET act together to establish an emergent microtubule and RAB-vesicle-dependent RET-SRC-EGFR-FGFR signaling hub. We demonstrate that drugs designed to inhibit RET alone work poorly in KIF5B-RET-transformed cells. However, combining the RET inhibitor sorafenib with drugs that target EGFR, microtubules, or FGFR led to strong efficacy in both *Drosophila* and human cell line KIF5B-RET models. This work demonstrates the utility of exploring the full biology of fusions to identify rational therapeutic strategies.

INTRODUCTION

Approximately 1.3 million new cases of non-small-cell lung cancer (NSCLC) patients are identified each year, comprising 80% of primary lung cancers (McCoach and Doebele, 2014). The prognosis for advanced and metastatic NSCLC patients is poor (Jemal et al., 2010). The identification of specific genetic alterations in large cohorts of NSCLC patients (e.g., KRAS and epidermal growth factor receptor [EGFR]) has yielded a potential avenue for matching treatments (e.g., RAS and EGFR pathway inhibitors) to specific groups of patients. Inhibition of these pathways using tyrosine kinase inhibitors (TKIs) have led to some clinical benefits, indicating the importance of stratifying patient populations based on driving genetic alterations (Pao et al., 2004).

Multiple gene fusions involving the rearranged-during-transfection (RET) kinase have been identified in lung adenocarci-

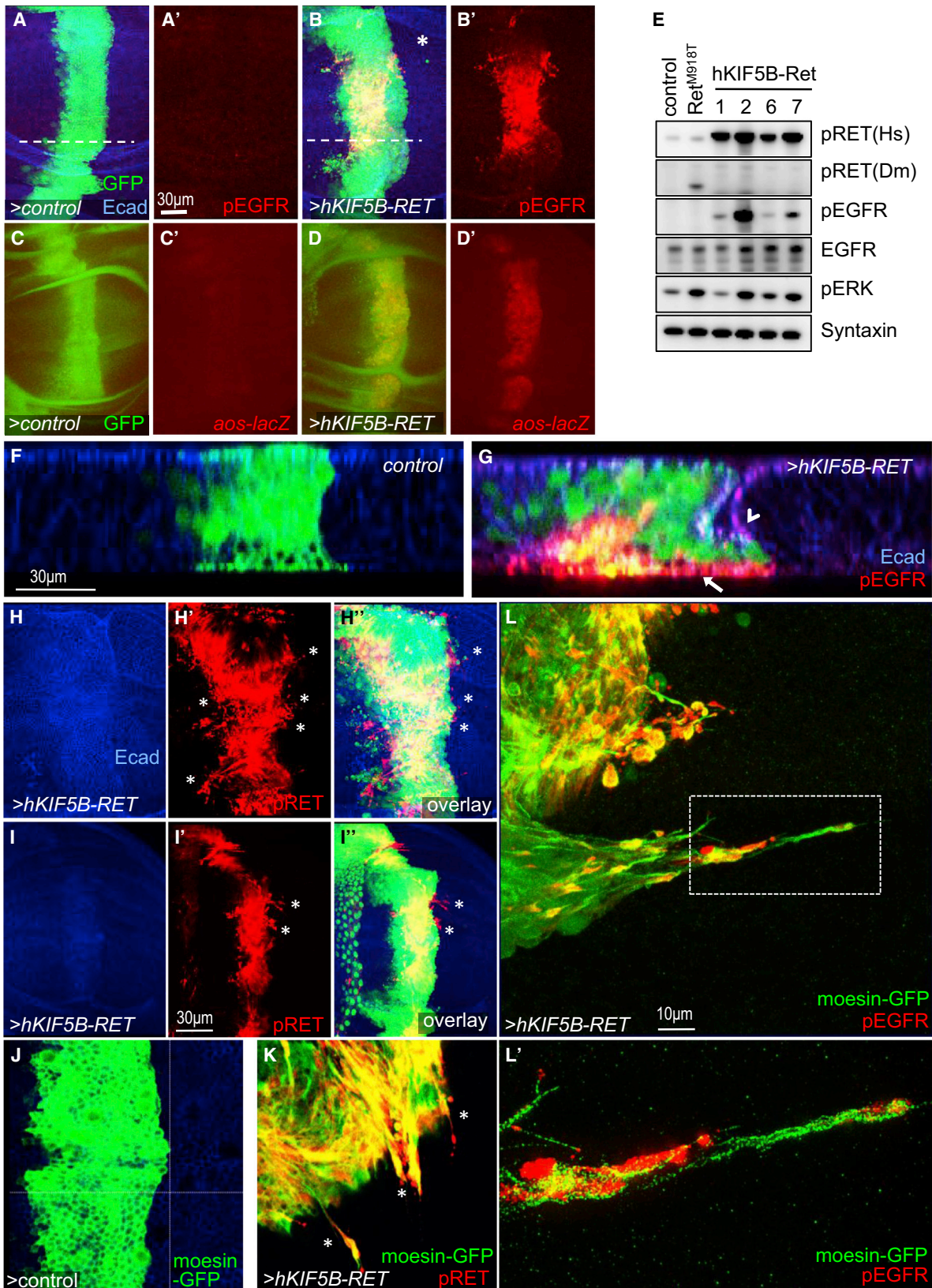
noma (LADC) patients, including KIF5B-RET, NCOA4-RET, and CCDC6-RET (Ju et al., 2012; Kohno et al., 2012; Lipson et al., 2012; Takeuchi et al., 2012). KIF5B-RET fusions account for approximately 2% of all NSCLC patients, primarily nonsmokers whose tumors exhibit few other genetic changes in known cancer drivers (Takeuchi et al., 2012). Efforts to treat patients with KIF5B-RET fusion driver oncogenes are focused on RET pathway inhibition, with eight active ongoing NSCLC clinical trials (McCoach and Doebele, 2014). However, our previous *Drosophila* studies indicated that the RET fusions NCOA4-RET and CCDC6-RET act through different signaling pathways and respond to different anti-cancer drugs, indicating functional differences that may affect patient treatment (Levinson and Cagan, 2016). The nature of the differences among activating point mutant RET isoforms, including RET fusions, is unknown.

In this study, we find that KIF5B-RET's C-terminal RET kinase domain activates canonical signaling pathways, while its N-terminal KIF5B domain activates multiple receptor tyrosine kinases (RTKs), including EGFR and fibroblast growth factor receptor (FGFR) signaling. The result is an emergent network that best responds to multi-targeting therapeutic cocktails. Therapeutics for other kinase fusion oncogenes may benefit from understanding the signaling pathways activated by each portion of the protein and how they act in concert to direct a unique transformation network.

RESULTS

Human KIF5B-RET Activates EGFR Signaling in a *Drosophila* Model

We cloned a patient-derived KIF5B-RET cDNA (Kohno et al., 2012) into an upstream activating sequence (UAS)-based expression vector, allowing us to target expression of the UAS-KIF5B-RET transgene to various fly tissues using the binary GAL4-UAS system (Figure S1E). Uniform KIF5B-RET expression in the third instar larval wing epithelium (wing disc) with a 765-GAL4 driver (765>KIF5B-RET) (Figure S1B) led to adult wings with multiple ectopic veins, which is indicative of elevated RAS/mitogen-activated protein kinase (MAPK) signaling (Karim and Rubin, 1998). 765>KIF5B-RET's ectopic venation phenotype was stronger than similarly targeted expression of wild-type human RET (described later) or expression of the *Drosophila* oncogenic ortholog dRET^{M955T} (765 > dRET^{M955T}), a constitutively activating point mutant RET variant commonly observed in medullary thyroid carcinoma patients



(legend on next page)

(Beldjord et al., 1995). Control flies displayed normal wing venation (Figures S1A–S1C). We conclude that human *KIF5B-RET* is capable of strongly activating the RAS/MAPK signaling pathway, a primary downstream effector of signaling by RET and other RTKs. Consistent with this view, RET activity was elevated in western blot analyses using an antibody to phosphorylated RET (pRET) (Figure 1E).

EGFR signaling is an axis of the RAS/MAPK cascade that regulates wing vein development (Martín-Blanco et al., 1999). Expressing the *KIF5B-RET* transgene in a stripe of cells at the center of the wing disc (*ptc>KIF5B-RET*) led to a strong upregulation of EGFR activity in vivo, as assessed with an antibody to activated, phosphorylated EGFR (pEGFR) (Figure 1B). Control and *ptc > dRET^{M955T}* (Figure S1D) flies did not show similar upregulation of the pEGFR signal. In *Drosophila*, EGFR signaling activates transcription of downstream targets, including *argos* and *pointed*. Wing discs expressing *ptc>KIF5B-RET* displayed in vivo upregulation of β -galactosidase reporters for each of these genes (*aos-lacZ*, Figures 1C and 1D; *pnt-lacZ*, Figures S1F and S1G), indicating that upregulation of EGFR activity led to activation of its canonical downstream signaling. In addition, *765>KIF5B-RET* wing discs showed strong upregulation of pEGFR by western blot analysis (Figure 1E). Knockdown of *Drosophila* EGFR can suppress the vein-thickening phenotype (*ptc>KIF5B-RET*; *EGFR^{RNAi}*) (Figures S1I and S1K) in *KIF5B-RET* cells, indicating EGFR activation by *KIF5B-RET* has functional outcomes. Altogether, these data indicate that *KIF5B-RET*—in contrast to *RET^{M918T}*—directs a complex signaling mechanism that includes activation of EGFR. To understand how *KIF5B-RET* and EGFR work together to promote transformation, we explored their subcellular localization.

KIF5B-RET Localizes EGFR to Filopodia- and Invadopodia-like Processes

Expression of *KIF5B-RET* in wing epithelial cells led to these *ptc>KIF5B-RET* cells shifting basally, an indication that they are undergoing an epithelial-to-mesenchymal transition similar to our previous SRC- and RET-based models (Figure 1G) (Dar et al., 2012; Vidal et al., 2006). Distinct from these models, however, *ptc>KIF5B-RET* cells extended long processes into the neighboring region of wild-type cells (Figures 1H and 1I), a phe-

nomenon not observed in control tissue (Figure 1F and 1J). The pRET immunofluorescence signal was detected along the length of these processes (Figures 1H and 1I, asterisks).

To more precisely analyze distribution of *KIF5B-RET* and EGFR, we coexpressed GFP-tagged Moesin (*ptc > moesin-GFP,KIF5B-RET*), an actin-binding protein that outlines cellular processes. Using high-resolution fluorescence microscopy, we found that pRET, pEGFR, and pSRC (Figures 1J–1L' and 4E) were present throughout the filopodia-like processes. Confocal z stacks indicated that pEGFR protein was also enriched basally in *ptc > moesin-GFP,KIF5B-RET* cells that had moved basally (Figure 1G).

Thus, *KIF5B-RET*-expressing cells displayed the presence of cellular processes indicative of migratory and invasive properties, including filopodia- and invadopodia-like structures enriched with active EGFR and RET receptors. We next investigated whether *KIF5B-RET* activated canonical RET pathways and whether other features of cellular transformation were present.

KIF5B-RET Activates Canonical RET Signaling through SRC

Previous work, including our own, has shown that activating point mutant RET isoforms promote signaling partly through the SRC signal transduction pathway (Dar et al., 2012; Liu et al., 2004; Read et al., 2005). Wing cells expressing *ptc>KIF5B-RET* strongly and cell-autonomously upregulated pSRC, activity as assessed with a pSRC-specific antibody (Figures 2B and 2J); pSRC was localized to the basal region of the epithelium (Figure 2D). EGFR and SRC are associated with invadopodia-like structures in migrating or metastatic cancer cells (Mader et al., 2011). *KIF5B-RET*-expressing cells showed upregulation and basal localization of Arp3 (Figures 2E and 2F), a key structural component of invadopodia (Clark et al., 2007). Thus, *KIF5B-RET* activated and localized pSRC, pEGFR, and ARP3—central components of invadopodia—to basal regions of the epithelium. We next investigated whether other aspects of transformation were altered, including degradation of basal lamina and cell polarity. Using a fly strain harboring a Collagen-GFP fusion transgene (Buszczak et al., 2007), we found that the basal lamina of *KIF5B-RET*-expressing cells was strongly

Figure 1. KIF5B-RET Activates and Localizes EGFR to Filopodia- and Invadopodia-like Processes

(A and B) Third instar larval wing epithelia, en face view. Expression of human *KIF5B-RET* in a central stripe of cells (*ptc>hKIF5B-RET*, marked by EGFP expression) resulted in upregulation of pEGFR levels. Some *KIF5B-RET*-expressing cells migrated away (B, asterisk) from the *ptc* region where the oncogene was expressed. Immunofluorescence images are composite overlays of z stacks spanning the full depth of the epithelia. In subsequent figures, *hKIF5B-RET* is referred to as *KIF5B-RET*. The dotted line shows the region for which the lateral view of the z series is shown in (F) and (G).

(C and D) Expression of *ptc>hKIF5B-RET* led to strong expression of EGFR activity reporter *aos-lacZ* compared to controls. Anti- β -galactosidase antibody was used to detect reporter activity.

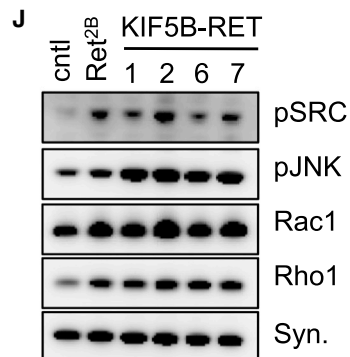
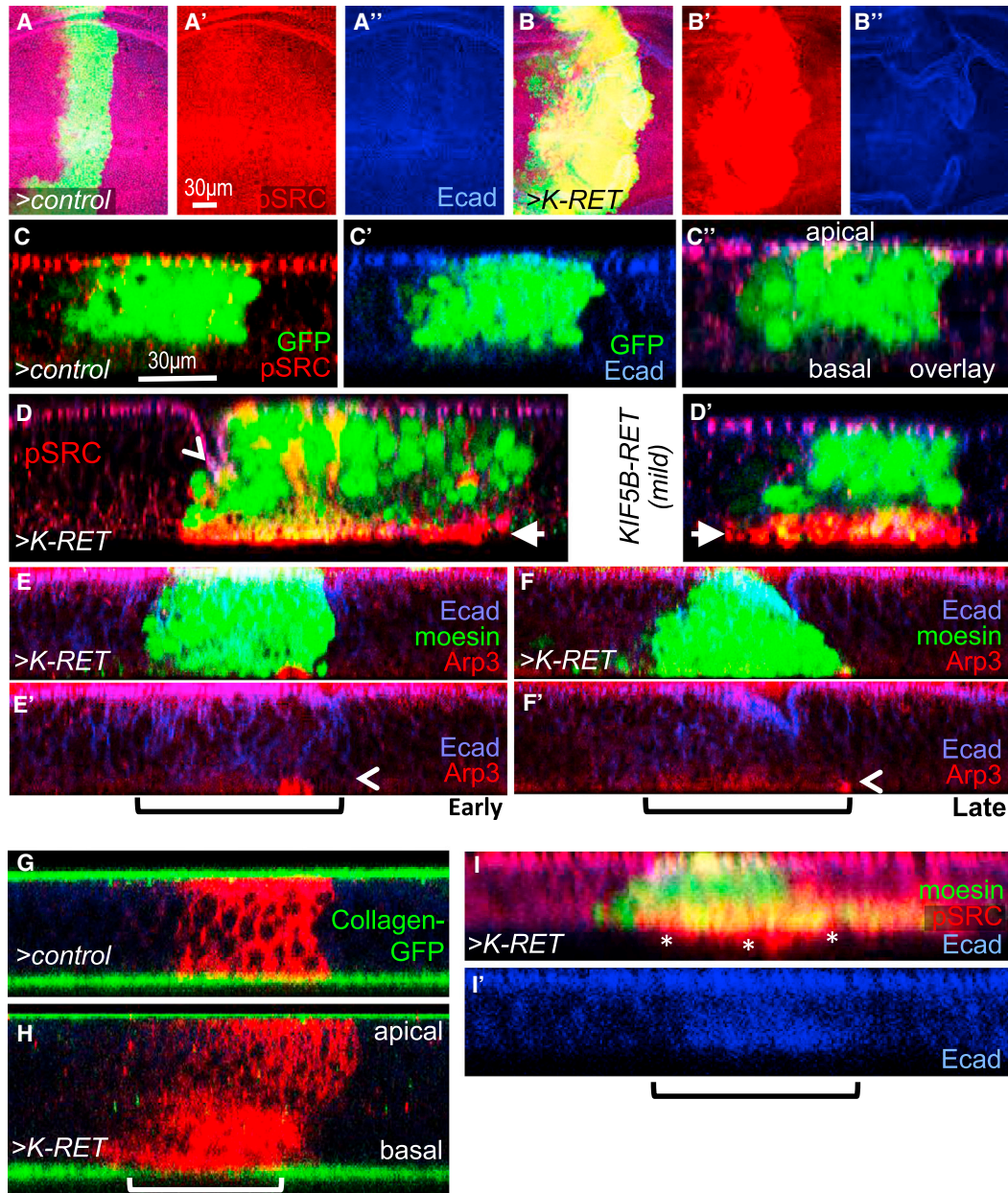
(E) Western blot of developing wing epithelia of the indicated genotypes; syntaxin was used as loading control. Four independent *KIF5B-RET* transgenic lines (*765>KIF5B-RET*) showed upregulation of pRET, pEGFR, total EGFR, and pERK levels. Expression of activating point mutant RET (*765 > dRET^{M955T}*) did not show upregulation of pEGFR.

(F and G) Many *ptc>KIF5B-RET* cells extruded basally and showed basal enrichment of the pEGFR signal (G, solid arrow). The arrowhead indicates invagination of epithelia as cells extrude basally. Lateral view of z series showing the full depth of epithelia. E-cadherin marks the apical region.

(H and I) *ptc>KIF5B-RET* cells displayed filopodia-like processes enriched with the pRET signal. These processes can extend laterally beyond *KIF5B-RET*-expressing cell bodies marked by GFP (H', H'', I', and I'', asterisks). Examples of especially long processes (I' and I'', asterisks).

(J and K) In *KIF5B-RET* cells, the pRET signal is localized throughout the filopodia-like processes (K, asterisks). Processes are visualized by cytoskeletal marker Moesin fused to GFP (*ptc > moesin-GFP,KIF5B-RET*).

(L) High-resolution microscopy shows the pEGFR signal is also enriched in these laterally projecting filopodia-like processes. A higher-magnification view (L') shows that the pEGFR signal extends to the distal ends.



(legend on next page)

degraded in contrast to controls or adjacent wild-type cells (Figures 2G and 2H). KIF5B-RET-expressing cells also showed loss of polarity: E-cadherin, which is normally present primarily in the apical regions of epithelia, was delocalized (Figure 2I). Western blot analysis of wing epithelium expressing KIF5B-RET showed upregulation of cell motility regulators' pJNK, RAC1, and RHO1 levels (Figure 2J; Figures S1L and S1M).

Altogether, KIF5B-RET signaling alters key aspects linked to cellular transformation. KIF5B-RET expression led to elevated activity of canonical RET signaling effectors, including SRC, but also upregulated at least one additional pathway, EGFR. We therefore explored how different KIF5B-RET structural domains contributed to each of these activities.

The KIF5B-RET Motor Domain Regulates pEGFR and pFGFR Activation

We used deletion- and point mutation-based structure and function studies to explore how each domain contributes to the complex mechanisms by which KIF5B-RET promotes transformation. The KIF5B-RET fusion protein consists of three major structural domains: motor, coiled coil, and kinase. We generated three KIF5B-RET variant fly models— Δ MMD (kinesin motor domain deletion), Δ CC (coiled-coil domain deletion), and 3Y-3F (tyrosine to phenylalanine changes of the three key residues 905, 1015, and 1062)—within the kinase domain of RET (Figure 3I) (Plaza-Menacho et al., 2014). Each domain was fused to the inducible UAS promoter, and each UAS transgene—including KIF5B-RET and RET controls—was targeted to the same genomic site using the *attP* system to ensure similar expression levels (Groth et al., 2004).

In these models, we evaluated the state of RET activation (pRET), canonical RET signaling (pSRC), and emergent KIF5B-RET signaling (pEGFR). While *ptc>KIF5B-RET* showed strong activation of these three markers (Figure 3B–3B''), removing the motor domain (*ptc>KIF5B-RET[Δ MMD]*) led to complete loss of the detectable pEGFR signal (Figure 3C'). Deletion of the motor domain also resulted in loss of pERK levels, as assessed by western blot analysis (Figure 3J). This indicated that the kinesin motor domain is primarily required for KIF5B-RET to activate EGFR and downstream MAPK signaling. *ptc>KIF5B-RET[Δ MMD]* wing epithelia still retained significant but reduced pRET levels (Figure 3C), suggesting that the high levels of pRET and pSRC activity observed in KIF5B-RET cells depend on recruitment and activation of EGFR through the motor domain.

Inactivating the kinase domain (*ptc>KIF5B-RET[3Y-3F]*) (Figures 3E–3E'') or removing the coiled-coil domain (*ptc>KIF5B-RET[Δ CC]*) (Figures 3D–3D'') led to loss of all three markers, indicating that dimerization through the coiled-coil domain and an active RET kinase domain were essential for full KIF5B-RET activity (also see Figure 3J). Activation of other downstream pathways, as measured by pERK, pJNK, and RAC1 levels, was also downregulated in both KIF5B-RET[3Y-3F] and KIF5B-RET[Δ CC] variants (Figure 3J).

We next tested whether other RTKs were recruited to this complex. KIF5B-RET upregulated activated FGFR (pFGFR) levels (*ptc>KIF5B-RET*) (Figures 3B''' and 3J), as well as total levels of the *Drosophila* PDGFR/VEGFR ortholog (Pvr) (western blot, Figure S2A). We restricted our analysis to RTKs for which working phospho-specific antibodies in *Drosophila* were available, i.e., pEGFR and pFGFR (Gibson et al., 2012). Activation of pFGFR was also dependent on the kinesin portion of the fusion protein (Figures 3C''' and 3D'''), as well as the kinase domain of RET (Figure 3E'''). The strong activation and localization of multiple RTKs (pEGFR and pFGFR) by KIF5B-RET was unique, because two RET fusions implicated in different cancers did not show similar upregulation of these pathways. CCDC6-RET activated pRET, pSRC, and pFGFR weakly and did not activate pEGFR (Figures 3G–3G''' and 3K) while NCoA4-RET activated all three markers moderately (Figures 3H–3H''' and 3K). None of these other RET fusion proteins provoked formation of filopodia or invadopodia processes (Figures 3G, 3H, and 3K).

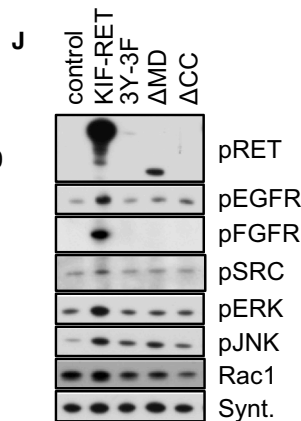
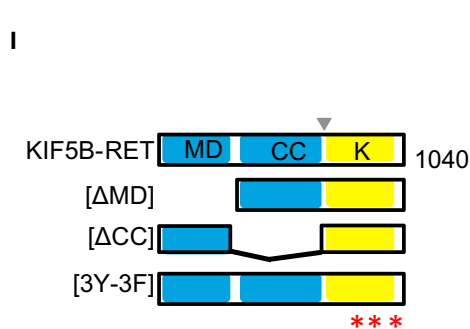
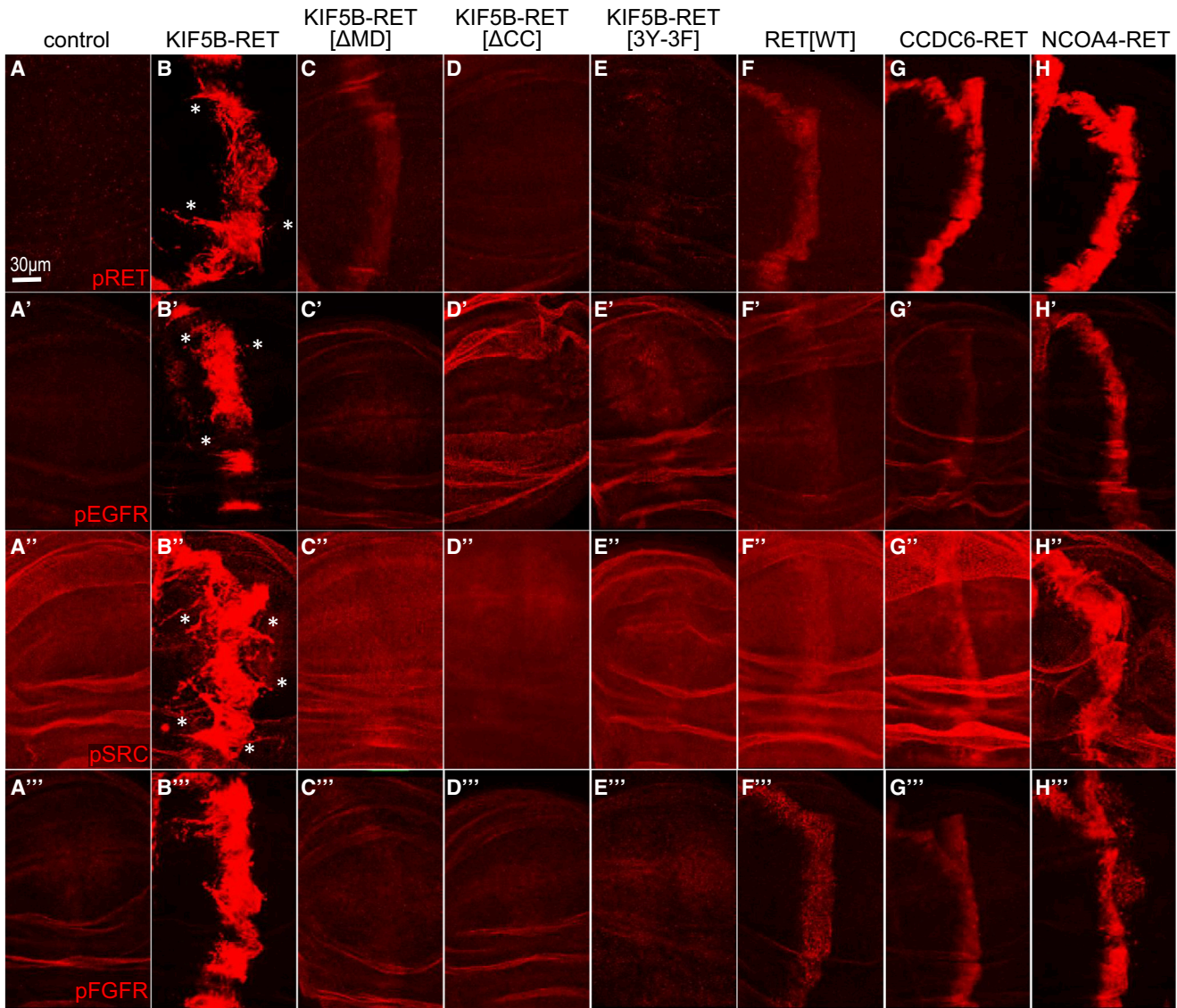
The failure of *ptc>KIF5B-RET[3Y-3F]* to activate EGFR, SRC, and FGFR is especially notable, indicating that RET kinase domain activity is required to establish a multi-kinase RET-SRC-EGFR-FGFR signaling hub. That is, the RET kinase domain acts with EGFR, FGFR, and SRC to mediate the full range of KIF5B-RET signaling. The requirement of pEGFR and pFGFR for an intact motor domain also suggested a novel multi-RTK signaling mechanism dependent on the kinesin domain, a possibility we explored.

KIF5B-RET Regulates pEGFR and pFGFR through RAB GTPases

Kinesin motor domain proteins transport cargo to distant cellular sites, including signaling effectors such as GRB2 and RAB vesicles (Hirokawa et al., 2009). RAB vesicles regulate RTK recycling and internalization; kinesin motors help deliver these kinase-vesicle complexes to specific sites for localized signaling

Figure 2. KIF5B-RET Activates Canonical RET Signaling through SRC

(A and B) *ptc>KIF5B-RET* cells (B) showed strong upregulation of the pSRC signal compared to controls (A) in third instar larval wing epithelium. (C and D) In control cells, pSRC was localized to apical regions of epithelia, overlapping E-cadherin. In *ptc>KIF5B-RET* cells, pSRC relocated to strongly accumulate in basal regions (arrowheads) of epithelia. Lateral z series view. (E and F) *ptc>KIF5B-RET* cells showed localized upregulation (E) or uniform upregulation (F) of Arp3 in basal regions. The arrowhead indicates the basal region; the bracket indicates the region expressing *KIF5B-RET*. (G and H) *ptc>KIF5B-RET* cells showed strong reduction of the basal lamina signal compared to control cells, as visualized with Collagen-GFP and MyR-RFP. The bracket indicates RFP-positive *ptc>KIF5B-RET* cells associated with reduced basal lamina. The Collagen-GFP signal in the apical region is from overlying peripodial epithelia. (I and I') *ptc > moesin-GFP, KIF5B-RET* cells showed loss of polarity: E-cadherin was no longer localized to apical adherens junctions and instead was distributed uniformly within cells. Compare with (C). pSRC was enriched in processes extending beyond basal lamina (I, asterisks). The bracket indicates the region of *KIF5B-RET* cells. (J) Western blot of developing wing epithelia of the indicated genotypes. Compared to control, four independent *KIF5B-RET* transgenic lines (*765>KIF5B-RET*) showed upregulation of pJNK, pSRC, Rac1, and Rho1.



K

	pRET	pEGFR	pSRC	pFGFR	Invadopodia/ filopodia
KIF5B-RET	+++	+++	+++	+++	+++
CCDC6-RET	++	-/+	+	+	-
NCOA4-RET	++	+	++	++	-
RET-WT	+	-	-/+	+	-

Figure 3. KIF5B-RET Motor Domain Regulates pEGFR and pFGFR Activation

(A–A''') Control cells showed basal levels of pRET, pEGFR, pSRC, and pFGFR signals in developing wing epithelia. (B–B''') *ptc>KIF5B-RET* cells showed strong upregulation of all four markers.

(legend continued on next page)

(Hirokawa et al., 2009). We identified a panel of 16 kinesin cargo adaptor molecules, including eight RAB proteins, and by targeted knockdown, assessed whether they are required to recruit and activate pEGFR and pFGFR (Figure 4A; Figure S2B) (Hirokawa et al., 2009).

We assessed requirement of these genes for KIF5B-RET function using a previously developed quantitative *Drosophila* viability assay (Dar et al., 2012). Expression of oncogenic KIF5B-RET in multiple developing tissues (*ptc>KIF5B-RET*) led to highly penetrant pupal lethality: only 2.3% of developing animals eclosed as adults. We found that RNAi-mediated knockdown of components of the Src-invadopodia complex and of individual *rab* genes increased the number of *ptc>KIF5B-RET* animals reaching adult stages (Figure 4A); this indicated that RAB proteins normally function to promote KIF5B-RET activity. Knockdown of RAB vesicles could in principle affect trafficking of different RTKs, and knockdown of Ret, Pvr, FGFR, and InR increased adult eclosion rates (Figure 4A).

Focusing on the key *rab* gene *rab9*, knockdown (*ptc>KIF5B-RET, rab9^{RNAi}*) led to strong reduction of KIF5B-RET-mediated pEGFR and pFGFR activation, indicating that the RAB machinery is involved in the recruitment and activation of pEGFR and pFGFR (Figures 4B–4C''; Figure S2C). Knockdown of *rab9* significantly reduced pSRC levels, but knockdown of EGFR, FGFR, and the other tested RTKs had mild effects on pSRC (Figure S2D) and pRET levels (Figure S2E). This suggested that removal of individual RTKs bound to KIF5B-RET had little effect on pSRC activation but simultaneous removal of multiple RTKs (pEGFR, pFGFR, etc.), e.g., through *rab9* knockdown, compromised pSRC activation. These data, together with our structure-activity-relationship (SAR) analysis, indicated that the KIF5B-RET molecule had a bipartite function: the RET kinase domain function (pSrc activation) could be uncoupled from the kinesin domain function (pEGFR and pFGFR activation), but there was mutual dependence of these kinase molecules to establish full activity of KIF5B-RET.

Knockdown of another kinesin adaptor protein, glutamate receptor interacting protein 1 (GRIP1) (Setou et al., 2002) also increased survival of *ptc>KIF5B-RET* flies to adulthood (Figure 4A). GRIP1 knockdown also resulted in loss of pEGFR activation by KIF5B-RET (Figures 4F and 4J); levels of pSRC and pRET were not affected, uncoupling EGFR and SRC activation (Figures 4D, 4E, 4H, and 4I). GRIP1 knockdown did not affect pFGFR activation, indicating that recruitment of pFGFR relies on an as-yet-unknown adaptor protein (Figures 4G and 4K). GRIP1 knockdown also suppressed aspects of EMT, including cell polarity as assessed by restoration of proper E-cadherin

localization, providing further evidence that the GRIP1-EGFR axis is functionally required for KIF5B-RET-mediated transformation (Figures 4L and 4M). GRIP1 has been previously implicated in modulating EGFR function in human cells (Yokomaku et al., 2005), and our findings extend these observations to KIF5B-RET.

Altogether, our fly studies support a model in which the KIF5B-RET fusion protein recruits a multi-protein signaling hub through its KIF5B kinesin domain plus its RET kinase domain. This signaling hub includes cofactors and adaptors such as RAB proteins and GRIP1 that, through their association with KIF5B-RET's motor domain, serve as specific activators of multiple RTKs like EGFR and FGFR.

HBEC3[KIF5B-RET] Lung Cells Exhibit Multiple Aspects of Transformation

We developed a lung cancer cell line model to determine which aspects of this signaling hub observed in *Drosophila* were also relevant to KIF5B-RET-transformed human cells. To model LADC, we used HBEC3-KT cells, normal human bronchial epithelial cells immortalized with CDK4 and hTERT (Sato et al., 2006). Using the pLenti6 vector system (Invitrogen), we generated multiple independent stable HBEC3 transformants that expressed KIF5B-RET.

Independent HBEC3[KIF5B-RET] lines exhibited significant differences from the parental line: most parental HBEC3 cells died a few days after reaching confluence, whereas HBEC3 [KIF5B-RET] cells survived for several weeks (Figures 5A and 5B); in addition, transformants showed robust growth in the absence of serum, in contrast to parental cells (Figure 5C). Analysis of cell biological features indicated that HBEC3[KIF5B-RET] cells extended striking filopodia-like processes (Figure 5E), as well as large numbers of actin-rich puncta compared to parental cells (Figure 5J). Actin-rich puncta are characteristic of invadopodia and are used to measure the relative frequency of invadopodia (Hoshino et al., 2013). HBEC3[KIF5B-RET] cells displayed a 7-fold increase in invadopodia-like structures (Figure S3B), mirroring results in our *Drosophila* KIF5B-RET model.

Western blot analysis of HBEC3[KIF5B-RET] cells indicated upregulation of EMT markers N-cadherin and Slug (Figure 5G), phenocopying important aspects of our *Drosophila* model. Stem cell fate factor SOX2 controls genetic programs that drive tumorigenesis and cancer cell motility, including lung cancers (Boumahdi et al., 2014; Siegle et al., 2014). Some studies, including ours, have shown that SOX2 levels are often upregulated in cancer cells after therapeutic treatment (Rothenberg et al., 2015; T.K.D., J. Esernio, and R.L.C., unpublished data),

(C–C'') *KIF5B-RET(ΔMD)* construct activates pRET (C) but cannot activate pEGFR, pSRC, and pFGFR.

(D and E) *KIF5B-RET(ΔCC)* (D–D'') and *KIF5B-RET(3Y-3F)* (E–E'') variants failed to activate all four markers.

(F–F'') Expression of the intact human RET gene *RET(WT)* activates the three markers pRET, pSRC, and pFGFR only slightly above basal levels. It fails to activate pEGFR.

(G–G'') Expression of *CCDC6-RET* activated pRET, and weakly activated pSRC and pFGFR, but did not activate pEGFR.

(H–H'') Expression of *NCOA4-RET* activated all four markers moderately.

(I) Schematic of altered versions of the human *KIF5B-RET* transgene used in our structure-activity-relationship (SAR) studies. ΔMD, deletion of motor domain, aa's 2–324; ΔCC, deletion of coiled-coil domain, aa's 324–582; 3Y-3F, tyrosine residues 905, 1016, and 1062 altered to phenylalanine. The arrowhead indicates the point of gene fusion; asterisks indicate point mutations within the kinase domain.

(J) Western blot of developing whole wing discs (*765>KIF5B-RET*) expressing different variants of *KIF5B-RET*.

(K) Summary table comparing three RET fusion isoforms with WT-RET and their ability to activate the four markers and induce filopodia or invadopodia.

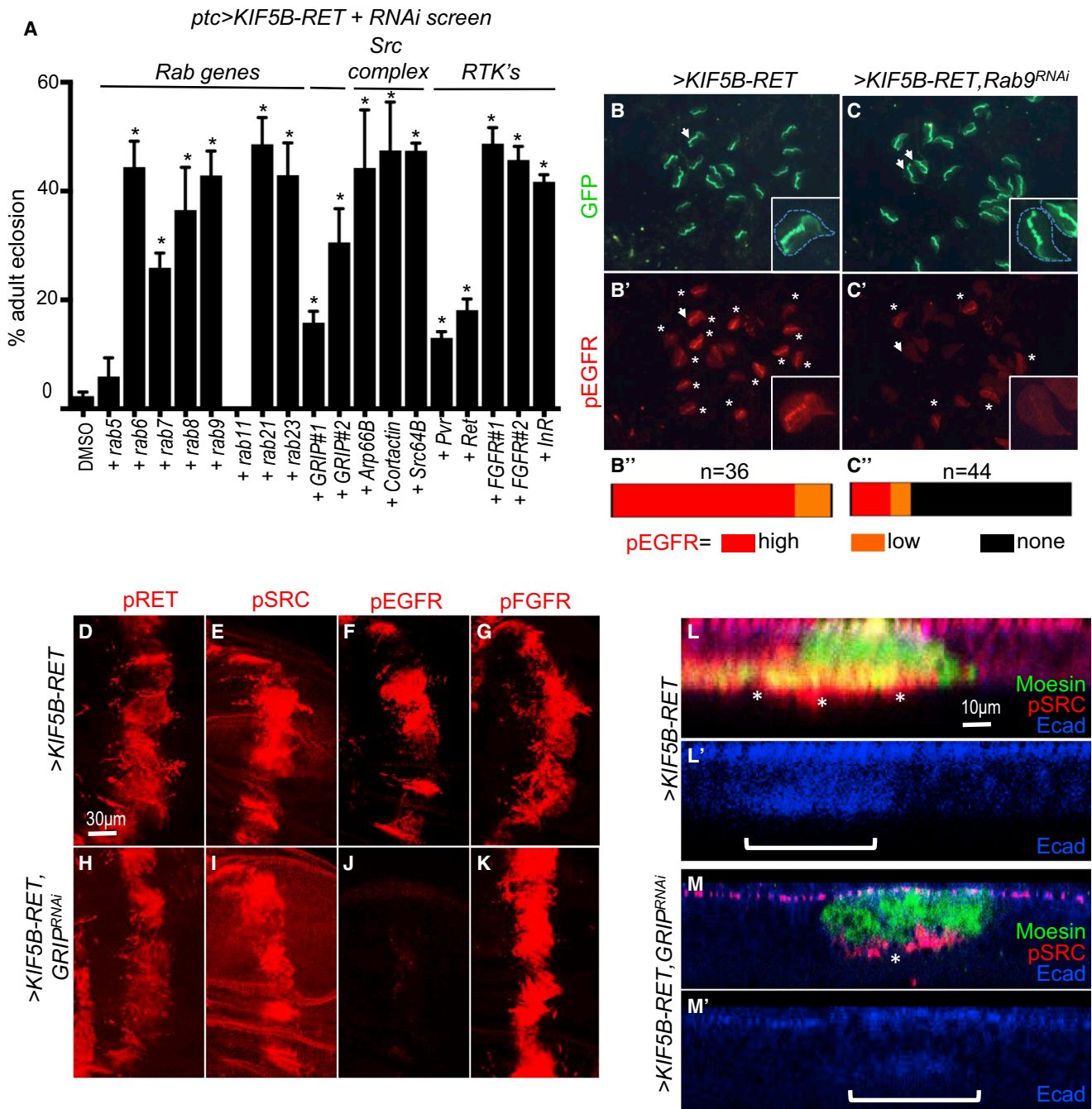


Figure 4. KIF5B-RET Regulates pEGFR through RAB GTPases and GRIP1

(A) Quantitative viability tests to assess whether reducing specific KIF5B-RET pathway components suppresses pupal lethality induced by *ptc>KIF5B-RET*. Percentage viability (eclosion) represents the number of adults that eclose after 12–14 days divided by the total number of embryos originally present (n). Asterisks indicate significance at $p < 0.05$ for each genotype compared to DMSO control using Student's t test with Welch's correction. Error bars represent SEM here and in subsequent figures; see [Experimental Procedures](#). For each data point, *>KIF5B-RET* + genotype (n = total number of embryos analyzed): *KIF5B-RET_DMSO*(202), +*Rab5^{RNAi}*(255), +*Rab6^{RNAi}*(242), +*Rab7^{RNAi}*(218), +*Rab8^{RNAi}*(301), +*Rab9^{RNAi}*(218), +*Rab11^{RNAi}*(318), +*Rab21^{RNAi}*(257), +*Rab23^{RNAi}*(234), +*GRIP1^{RNAi}*(273), +*GRIP2^{RNAi}*(136), +*Arp66B^{RNAi}*(234), +*Cortactin^{RNAi}*(239), +*Src64B^{RNAi}*(313), +*Pvr^{RNAi}*(91), +*Ret^{RNAi}*(140), +*FGFR#1(btj)^{RNAi}*(366), +*FGFR#2(htj)^{RNAi}*(336), and +*InR^{RNAi}*(201).

(B and C) Low-magnification immunofluorescence images: in *ptc > eGFP, KIF5B-RET* wing discs, almost all discs showed strong activation of pEGFR (B', asterisks). Simultaneous knockdown of Rab9 (*ptc > eGFP, KIF5B-RET, Rab9^{RNAi}*) reduced the number of discs showing high pEGFR activation (C'). Representation of relative number of discs showing high, low, and no detectable pEGFR expression (B'' and C''), in which n represents the number of discs analyzed. Examples of wing discs in the insets are marked by the white arrowheads; the dotted line outlines the entire tissue.

(legend continued on next page)

suggesting a role for stem cell fate effectors in promoting tumorigenesis, as well as resistance to therapy. We found that SOX2 levels were strongly upregulated in multiple HBEC3[KIF5B-RET] cell lines compared to HBEC3 parental cells when grown to confluency (Figures 5G, 5K, and 5L). We conclude that KIF5B-RET promotes key aspects of cellular transformation in human bronchial epithelial cells.

HBEC3[KIF5B-RET] Cells Signal through Multiple Cancer-Related Axes

To explore the overall state of the HBEC3[KIF5B-RET] kinase network, we performed a phospho-kinase array analysis (Cell Signal PathScan RTK Signaling Array). HBEC3[KIF5B-RET] cells showed broader activation of kinases compared to parental cells (Figure 5F). Similar to our *Drosophila* KIF5B-RET models, pSRC levels were strongly upregulated. Phosphorylation of RTKs such as HER2, HER3, FGFR1, FGFR3, and FGFR4 were also upregulated, as was the phosphatidylinositol 3-kinase (PI3K) pathway effector AKT at two positions (471 and 304). We observed a strong downregulation of the RAS pathway effector pERK1/2 (see also Figure 5G).

Using western blot analysis, we confirmed modest increases in levels of the N-terminal region of KIF5B and phosphorylation of RET at position 1062 (pRET[Y1062]) (Figure 5H). RAB proteins RAB5, RAB7, and RAB9 were moderately upregulated within physiological levels (Figure 5H). We observed a significant increase in a SRC-dependent tyrosine phosphorylation in EGFR (pEGFR[Y845]); we observed a significant decrease in MAPK-dependent EGFR phosphorylation (pEGFR[Y1068]). This switch from ERK-dominant to SRC-dominant EGFR phosphorylation mirrors the overall changes in activity of these two cytoplasmic kinases (Figures 5F and 5G). These results raise an interesting mechanistic question: what components of the KIF5B-RET signaling hub regulate this ERK-to-SRC switch in signaling specificity?

HBEC3[KIF5B-RET] Cells Showed Cofactor-Dependent pEGFR Signal Switching

In situ immunofluorescence staining confirmed that HBEC3 [KIF5B-RET] cells grown to confluence exhibited increased pEGFR[Y845] and decreased pEGFR[Y1068]; conversely, parental cells exhibited low pEGFR[Y845] and high pEGFR [Y1068] levels (Figures 6A, 6B, 6E, and 6F). This further emphasizes a KIF5B-RET switch from ERK-dominant to SRC-dominant signaling. Removal of epidermal growth factor (EGF) from the growth media resulted in complete loss of the high basal pEGFR[Y1068] signal of parental cells (Figures S4D and S4E), indicating these phosphorylation sites are bona fide predictors of EGFR signaling.

We next performed small interfering RNA (siRNA)-mediated knockdown of components of the KIF5B-RET signaling hub to

establish their functional requirement. Using siRNA-directed knockdown on confluent HBEC3[KIF5B-RET] cells, reduction of GRIP1, SRC, or RAB9A all led to strong suppression of the increased pEGFR[Y845] signal induced by KIF5B-RET (Figures 6C and 6D; Figure S4C). In contrast, knockdown of these components moderately increased the pEGFR[Y1068] signal in HBEC3[KIF5B-RET] cells (Figures 6G and 6H; Figure S4G). Knockdown of GRIP1, SRC, or RAB9A in KIF5B-RET cells also led to reestablishment of high pERK levels (Figure 6I). Altogether, these data indicate that SRC, GRIP1, and RAB9A normally mediate KIF5B-RET-mediated switching of EGFR from predominantly phospho-Y1068 to predominantly phospho-Y845, that is, switching from an ERK-associated phosphorylation event to a SRC-associated event.

This switch in preferred EGFR phosphorylation sites distinguishes activating point mutant RET from KIF5B-RET. We explored ways to incorporate these findings to identify therapeutic approaches better tailored for suppressing KIF5B-RET-mediated transformation.

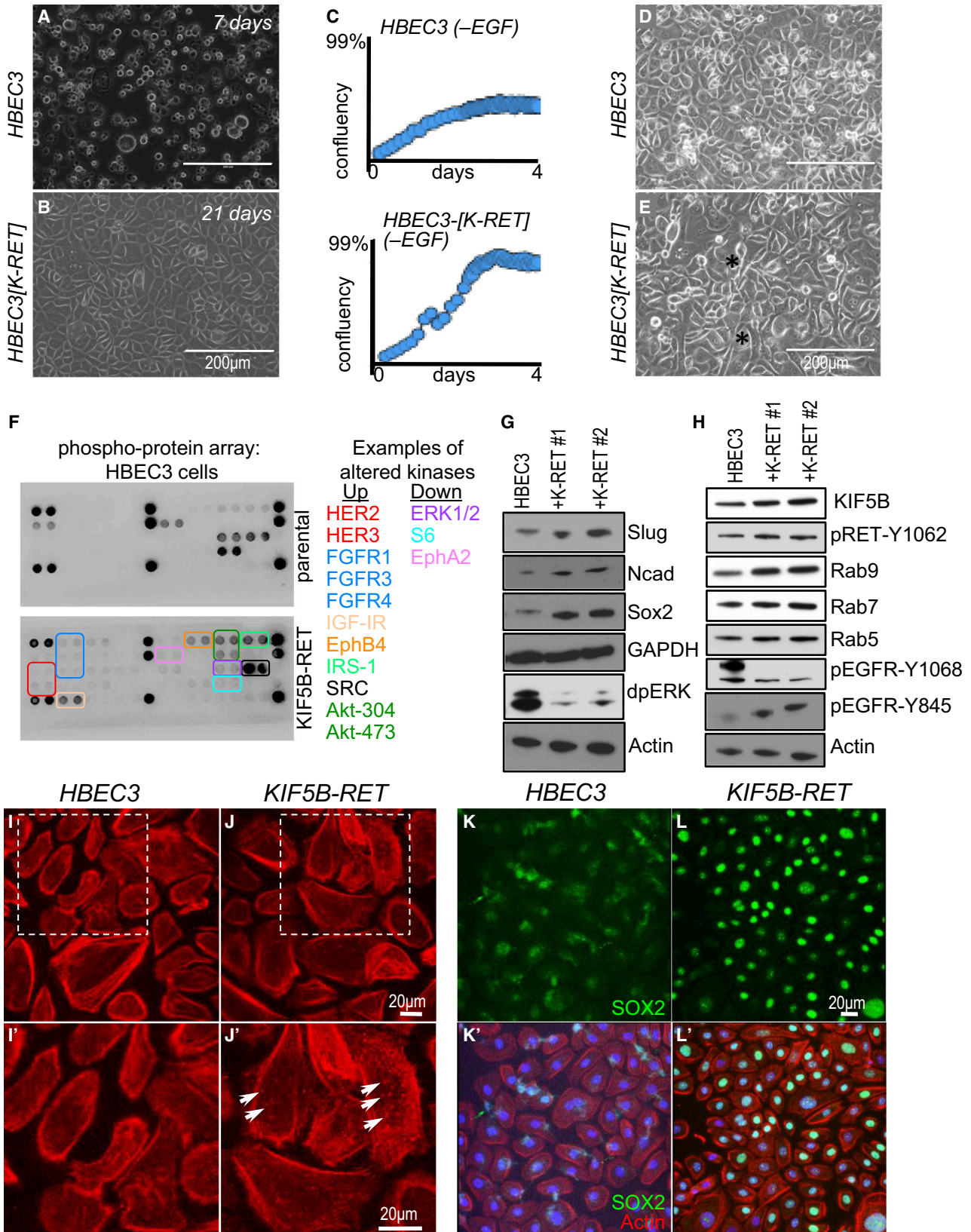
Inhibiting EGFR Signaling Improves Therapeutic Targeting of the KIF5B-RET Network

Using our fly viability assay, we screened a panel of 66 U.S. Food and Drug Administration (FDA)-approved drugs for their ability to rescue KIF5B-RET-induced pupal lethality (*ptc>KIF5B-RET*). The list (Figure S6) included the polypharmacological lead compound AD80, a kinase inhibitor previously demonstrated to inhibit RET and downstream signaling components (Dar et al., 2012). In this assay, AD80 showed the best efficacy profile, rescuing pupal viability from ~2% (controls) to ~70% viability (Figure 7A). The RET pathway inhibitors regorafenib and sorafenib and the MEK inhibitor trametinib were less effective, while FDA-approved drugs for RET-driven tumors, including vandetanib and cabozantinib, provided only marginal improvement in fly viability. HBEC3[KIF5B-RET] cells were also poorly responsive to vandetanib or cabozantinib (Figure 7C; Figures S7A and S7B), further indicating that canonical RET inhibitors are not effective in reducing KIF5B-RET-mediated transformation. Neither drug was as effective as the EGFR inhibitor erlotinib in confluent HBEC3[KIF5B-RET] cells (Figure 7C), again emphasizing the importance of EGFR in KIF5B-RET-mediated transformation.

To further assess the importance of inhibiting both RET and EGFR activity, we used fly wing discs as an in vivo assay: *ptc>KIF5B-RET* larvae were fed drugs orally, and larval wing epithelia were examined for pEGFR activity. Efficacy in flies and cell lines tracked with activity against EGFR: AD80 proved to be the most potent compound for inhibiting both pRET and pEGFR activation (Figures S5A and S5B). The FDA-approved drug sorafenib—in clinical trials for RET-based cancers (Lam et al., 2010)—also showed significant inhibition of pEGFR in vivo,

(D–K) Immunofluorescence images of wing discs showing the effect of *GRIP1^{RNAi}* knockdown on phospho-protein marker activation by *KIF5B-RET*. *ptc>KIF5B-RET* cells displayed high levels of pRET, pSRC, pEGFR, and pFGFR. Including knockdown of kinesin cofactor protein GRIP1 (*ptc>KIF5B-RET, GRIP1^{RNAi}*) did not alter pRET, pSRC, or pFGFR (H, I, and K) but strongly suppressed pEGFR activation (J).

(L and M) Knockdown of GRIP1 suppressed loss of polarity induced by *KIF5B-RET* expression. *ptc>KIF5B-RET* cells showed loss of localized apical E-cadherin and high levels of basally localized pSRC in distinct cellular processes (L, asterisk). Including knockdown of GRIP1 (*ptc>KIF5B-RET, GRIP1^{RNAi}*) maintained E-cadherin primarily in the apical region of the epithelia and showed low levels of pSRC that failed to strongly enrich in basal processes (M, asterisk).



(legend on next page)

though less inhibition than AD80 (Figure S5C). Fly tissues treated with AD80 still retained some pRET function (Figure S5B'') in vivo, highlighting the need for targeting other relevant pathways for optimal therapeutics.

Our *Drosophila* structure and function studies demonstrated a key, previously undescribed, requirement for KIF5B-RET function: kinesin domain-dependent EGFR activation. Kinesin motors depend on microtubules for cargo transport. We therefore tested clinically relevant microtubule inhibitors for their ability to inhibit EGFR activation. Microtubule inhibitors vincristine and paclitaxel moderately inhibited pEGFR activation (Figures S5D and S5E).

Addressing Multiple Pathways Improves Efficacy against KIF5B-RET Transformation

Polypharmacological lead compound AD80's targets include RET, SRC, and multiple EGFR targets, including BRAF and S6K. In addition, AD80 inhibits FGFR, PDGFR, VEGFR, and InR (Dar et al., 2012) targets that were genetically required for KIF5B-RET function in fly assays. AD80 provided the strongest rescue in our KIF5B-RET *Drosophila* survival assay (Figures 7A and 7B). The multi-kinase inhibitors AD80 and sorafenib also showed strong activity in confluent human HBE3[KIF5B-RET] cells: both showed strongly reduced IC₅₀ in HBE3[KIF5B-RET] cells compared to the parental line—especially in confluent cultures—indicating that KIF5B-RET has conferred a dependence on RET kinase signaling (Figure 7C; Figures S7A–S7C). AD80 was the most potent on low-confluency cells (Figure S7B).

One key difference between the experimental compound AD80 and the FDA-approved drug sorafenib is that sorafenib is a poor inhibitor of SRC (Apsel et al., 2008), the primary signaling axis activated by EGFR in the context of KIF5B-RET. One prediction is that sorafenib's efficacy would be enhanced by adding EGFR inhibitors such as gefitinib or erlotinib or by adding microtubule inhibitors like paclitaxel that inhibited pEGFR recruitment by KIF5B-RET. Rescue of sorafenib-treated *ptc>KIF5B-RET* flies was improved when treatment included gefitinib, matching levels of AD80 rescue; sorafenib also performed better in the presence of paclitaxel (Figure 7B). HBE3[KIF5B-RET] cells showed strongly increased sensitivity when sorafenib was combined with low-dose erlotinib (0.1 μM) or low-dose paclitaxel

(3 nM); AD80 showed little improvement when combined with erlotinib (Figure 7C; Figures S7A and S7B) (data not shown). While our manuscript was in submission, a study consistent with our findings showed that RET and EGFR inhibitor combinations worked well against some RET fusions (Vaishnavi et al., 2017).

Finally, the BRAF-inhibitor vemurafenib was less effective on HBE3[KIF5B-RET] cells than parental lines (Figure S7C), further highlighting the shift from pERK1/2 activation. In summary, our therapeutic studies indicate that combining available RET inhibitors with EGFR inhibitors or microtubule regulators can be a potent therapeutic strategy that better accounts for the unusual signaling networks activated by KIF5B-RET.

DISCUSSION

Gene fusions represent some of the earliest described genetic aberrations linked to cancer (Mertens et al., 2015). Targeting the kinase portion of the fusion protein has proved to be a useful strategy: for example, treating patients with a *BCR-ABL* fusion using Abl inhibitors provided the first example of a successful treatment with targeted therapy (Cohen et al., 2002). The therapeutic paradigm has focused primarily on targeting the kinase domain of the kinase fusion protein with TKIs. Model studies or patient trials in *ALK*, *ROS1*, *BRAF*, and *RET*– fusion-containing cancers have focused on driver-specific TKIs as a primary therapeutic strategy (Galetta et al., 2012); TKIs have been approved for *PDGFRB*– and *ALK*– fusion-containing epithelial tumors (Forde and Rudin, 2012; Wright and Petersen, 2007).

Our findings challenge this paradigm of therapeutics that solely target the kinase function of fusion oncogenes. Our studies have shown that (1) the N terminus of KIF5B-RET fusion protein recruits multiple RTKs; (2) the RET kinase domain depends on components such as SRC, GRIP1, and RAB9A for oncogenic signaling; (3) the assembled kinases form a multi-protein signaling hub in which they reinforce mutual phosphorylation; and (4) optimal therapy against KIF5B-RET requires inhibition of RET, SRC, EGFR, and FGFR (Figures 7D and 7E). Clinical trials of patients with RET fusions showed KIF5B-RET patients were less responsive to the RET inhibitor vandetanib (Yoh et al., 2017) compared to CCDC6-RET patients. In other

Figure 5. HBE3[KIF5B-RET] Lung Cells Exhibit Multiple Aspects of Transformation

(A and B) Phase contrast images of parental *HBE3* and stably transfected *KIF5B-RET* cells. Parental cells started dying after 7 days, while *KIF5B-RET* cells maintained cell-cell contacts and survived beyond 21 days.

(C) IncuCyte-based live imaging (every 6 hr) and confluency analysis. Parental *HBE3* cells (top panel) grew poorly in media lacking growth factor EGF, while *KIF5B-RET* cells (bottom panel) grew rapidly to reach confluency in 4 days.

(D and E) Phase contrast images of *KIF5B-RET* cells extending long filopodia-like processes (E, asterisks).

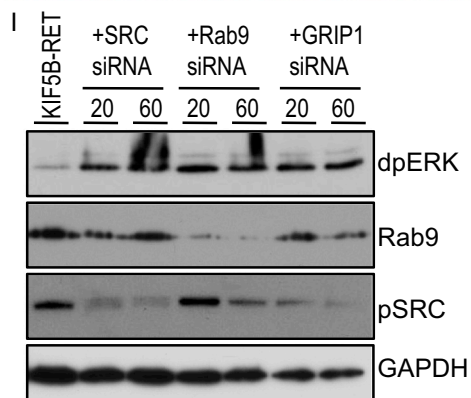
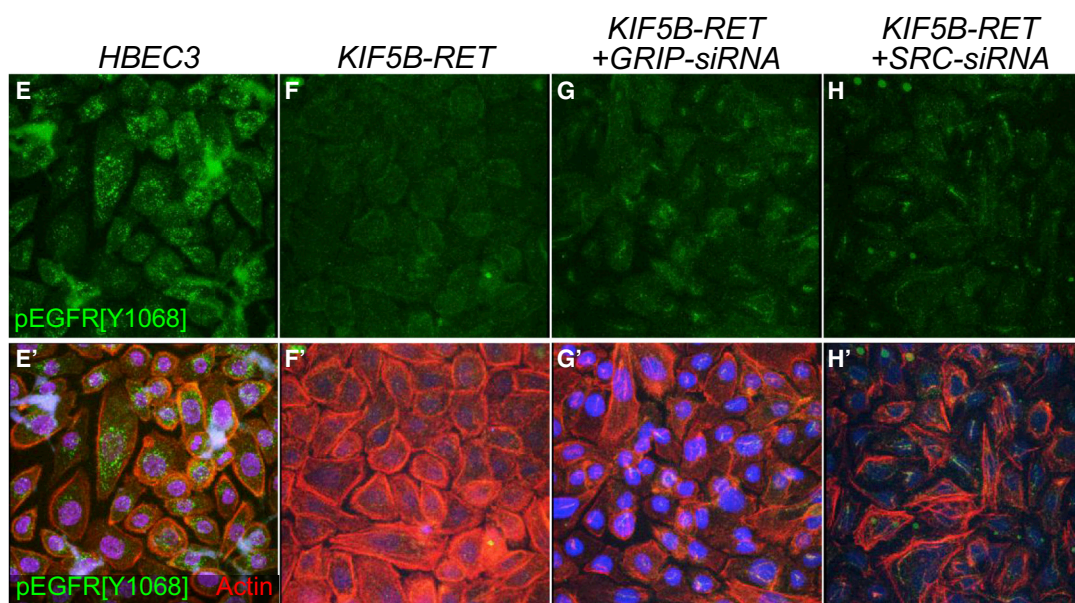
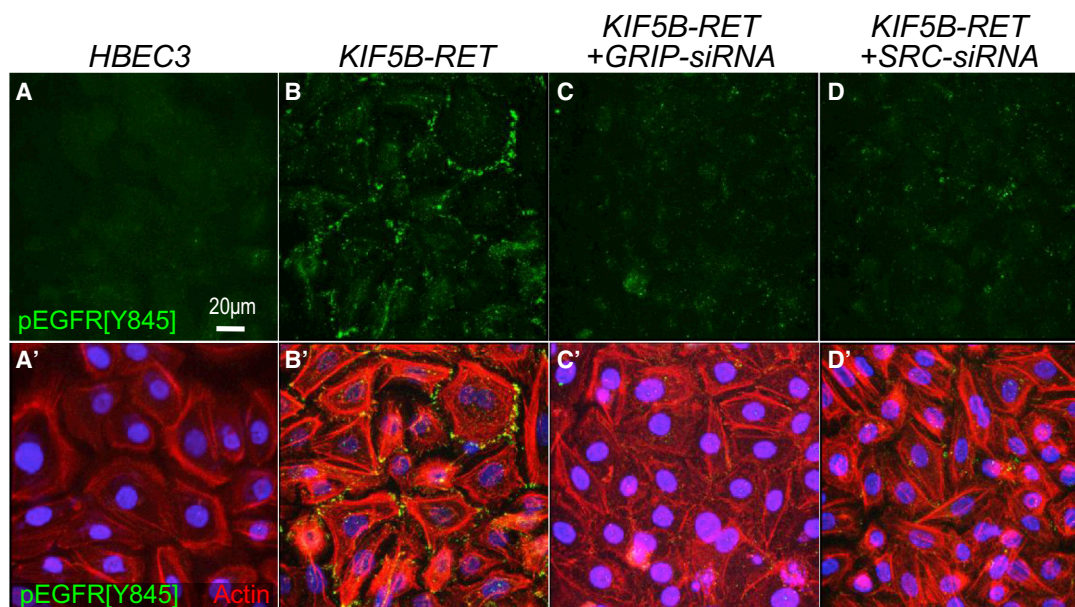
(F) Cell Signal PathScan RTK Signaling Antibody Array images of protein lysates from parental *HBE3* and *KIF5B-RET* cells. Examples of kinases deregulated in *KIF5B-RET* cells are provided as a list matched to colored boxes. The array list is in Figure S3A.

(G) Western blot of protein lysates from parental *HBE3* and two independent *KIF5B-RET*-transfected cell lines. *KIF5B-RET* cells showed upregulation of EMT markers Slug and N-cadherin and the protumorigenic stem cell marker Sox2. dpERK levels were reduced in *KIF5B-RET* cells.

(H) Western blot demonstrating that *KIF5B-RET*-transfected cell lines upregulate KIF5B and pRET[Y1062] levels within physiological levels. In addition, Rab9 and Rab7 were moderately upregulated, while Rab5 was more weakly upregulated. Regarding EGFR, pEGFR[Y845] was upregulated, while pEGFR[Y1068] was downregulated.

(I and J) Actin cytoskeleton of *KIF5B-RET*-transfected and parental cells visualized by phalloidin-rhodamine staining. *KIF5B-RET* cells contained a large number actin-rich puncta (arrows) characteristic of invadopodia. There was a 7-fold increase (Figure S3B) in actin-rich puncta in *KIF5B-RET* cells (median 15.5/cell) compared to parental *HBE3* cells (median 2.5/cell).

(K and L) *KIF5B-RET* cells showed strong upregulation of tumorigenic stem cell transcription factor Sox2 in the nuclei. Parental cells showed low levels of Sox2 that was mostly excluded from nuclei.



(legend on next page)

trials of RET fusion patients—using various RET inhibitors (Drilon et al., 2016; Gautschi et al., 2017)—the objective response of KIF5B-RET patients was consistently low, suggesting failure of single-agent RET inhibitor therapy. These clinical findings support our studies. In these trials, KIF5B-RET fusions represented the most common RET-rearranged events in LADC patients, suggesting a potentially significant impact of our therapeutic findings for treatment.

Our studies have also uncovered a mechanism whereby KIF5B-RET protein switches intracellular signaling from being pEGFR-Y1068/MAPK dominant to being pEGFR-Y845/SRC dominant (Figure 7E). Strong upregulation of pSRC and pEGFR in KIF5B-RET cells could likely increase the binding and affinity of EGFR to adaptors to potentiate downstream signaling (Begley et al., 2015) or promote invasive behavior in transformed cells (Mader et al., 2011). KIF5B-RET studies in mammalian cells have shown similar strong upregulation of the SRC pathway (Lin et al., 2016). In addition, analysis of a cohort of patients with KIF5B-RET rearrangement (Sarfaty et al., 2017) shows frequent visceral metastases, which is consistent with our findings of increased SRC-dependent local invasion through invadopodia formation.

With respect to the signaling hub promoting oncogenic signaling by KIF5B-RET, we propose that the identity of RTKs recruited by the RAB vesicle would depend on the cell type and KIF5B-RET fusions occurring in other cancers could potentially assemble a different palate of RTKs with different signaling outcomes, thus requiring different therapeutics. This could explain why, in contrast to published KIF5B-RET data, our studies using human lung cells identified this multi-RTK-containing signaling hub.

Finally, we have shown that KIF5B-RET signaling can be therapeutically inhibited by targeting RET, EGFR, FGFR, and SRC. Additional components of this hub, like the RAB and kinesin machinery, could be potentially targeted, opening additional therapeutic windows into treating KIF5B-RET tumors. This would be especially important because RABs and kinesins could be recruiting other, as-yet-unidentified signaling components into the KIF5B-RET signaling hub. Future studies can focus on whether additional components are recruited to this multi-protein signaling hub and the best therapeutic options for inhibiting them.

EXPERIMENTAL PROCEDURES

Antibodies and Histology

Third instar wing discs were staged and fixed in 4% paraformaldehyde. Immunofluorescence was performed as described (Das et al., 2013). The antibodies used were anti-pRET[Y905], anti-pJnk, anti-pAkt, anti-SOX2, anti-slug, anti-

N-cadherin, anti-pEGFR[Y845], anti-pEGFR[Y1068], anti-pFGFR[Y653/654], anti-Rab5, anti-Rab7, anti-Rab9 (Cell Signal), anti-pSRC[Y418] (Invitrogen), and anti-dpERK (Sigma), plus anti-actin, anti-E-cadherin, anti- α -Catenin, anti-Rho1, anti-syntaxin, anti- β -tubulin (Developmental Studies Hybridoma Bank), anti-actin, anti-GAPDH antibodies (Santa Cruz Biotechnology), anti-Rac1 antibody (BD Biosciences), anti-KIF5B (Abcam), anti-EGFR (Julia Cordero), and anti-Arp3 (William Theurkauf).

Comprehensive Statistical Analysis

For viability pupal analysis, in Figures 4 and 7, mean and SEM were calculated, and 4–5 vials per experiment, biological replicates, per dose were analyzed and repeated at least 2 times. Each vial had between 20 and 80 developing embryos, and the total (n) indicated in the legends represents the total number of embryos analyzed. For the large 66-drug library screen, 8 vials per drug, biological replicates, with approximately 20 pupae per vial were analyzed; the ratio of eclosed adults to pupae was plotted. To assess the statistical significance of the difference between means, a t test with Welch's correction was performed using PRISM software. The correction was used to account for samples with unequal variances and unequal sample sizes. For MTT on cancer cells, each dose was performed in quadruplicate and mean signal and SEM were analyzed.

Fly Stocks, Genetics, and Subcloning

Fly stocks were obtained from the Bloomington and Vienna *Drosophila* Resource Center (VDRC) *Drosophila* stock centers. *UAS-KIF5B-RET* flies were generated by cloning a human cDNA obtained from Dr. Ohno. For structure function analysis of human KIF5B-RET (hKIF5B-RET), variants were generated using standard molecular biology subcloning techniques and cloned into the pUAST-attB vector. RET-WT DNA was obtained from Dr. Plaza-Menacho. Injection and creation of attp40 transgenics was done by BestGene.

Inhibitor Studies in Flies

Drugs were obtained from LC Laboratories or Selleck Chemicals and were dissolved in DMSO as stock solutions ranging from 1 to 200 mM. Drugs (500–1,000 μ L) were diluted in molten (~50°C–60°C) enriched fly food and aliquoted into 5 mL vials. Drug concentrations represent final concentration in fly food. 30–60 embryos of each genotype were raised on drug-containing food until they matured as third instar larvae (wing disc western assay) or allowed to proceed to adulthood (viability assay and wing vein quantitation assay).

MTT Assay

Cancer cell lines were cultured in airway epithelial basal media supplemented with a bronchial epithelial growth kit from ATCC. Cells were grown in 75 cm² sterile polystyrene culture flasks to 80% confluency, trypsinized, and reseeded in equal aliquots into 96-well plates. After 2 days and ~50% confluency, media were removed and replaced with DMSO or drug-containing media. Cells were allowed to grow another 4 days (like other fast-growing cancer lines), after which MTT assay was performed. Spectrophotometric readings at 590 and 630 nm using a 96-well plate reader were used to establish growth and viability of cells. Each drug dose was tested in quadruplicate, and experiments were repeated twice.

Phospho-protein Array Analysis

The PathScan RTK Signaling Antibody Array Kit (Cat. No. 7982) was used to assess kinase activity of human cancer cell lines. Briefly, human cancer cells

Figure 6. HBE3[KIF5B-RET] Cells Show Cofactor-Dependent pEGFR Signal Switching

(A–D) Immunofluorescence images showing upregulation of pEGFR-Y845 levels in *KIF5B-RET* cells (B) compared to parental cells (A). siRNA-mediated knockdown of *GRIP1* (C) and *SRC* (D) suppressed the increase of pEGFR-Y845 levels in *KIF5B-RET* cells. DAPI labels nuclei, and phalloidin-rhodamine labels the actin cytoskeleton.

(E–H) Immunofluorescence images showing strong downregulation of pEGFR-Y1068 levels in *KIF5B-RET* cells (F) compared to parental cells (E). siRNA-mediated knockdown of *GRIP1* (G) and *SRC* (H) suppressed the effect of *KIF5B-RET* by moderately increasing levels of pEGFR-Y1068.

(I) Western blot of *KIF5B-RET* cells with knockdown of indicated genes. Numbers indicate final concentration of siRNA (in nanomolars) in media. While *KIF5B-RET* cells showed low levels of dpERK (lane 1; also see Figures 5F and 5G), knockdown of *SRC*, *RAB9A*, or *GRIP1* led to increased dpERK levels. *RAB9A* knockdown led to reduction of pSRC levels, similar to the fly experiments. *RAB9A* and *SRC* blot panels confirm that siRNA knockdown led to strong reduction in *RAB9A* and *SRC* levels.

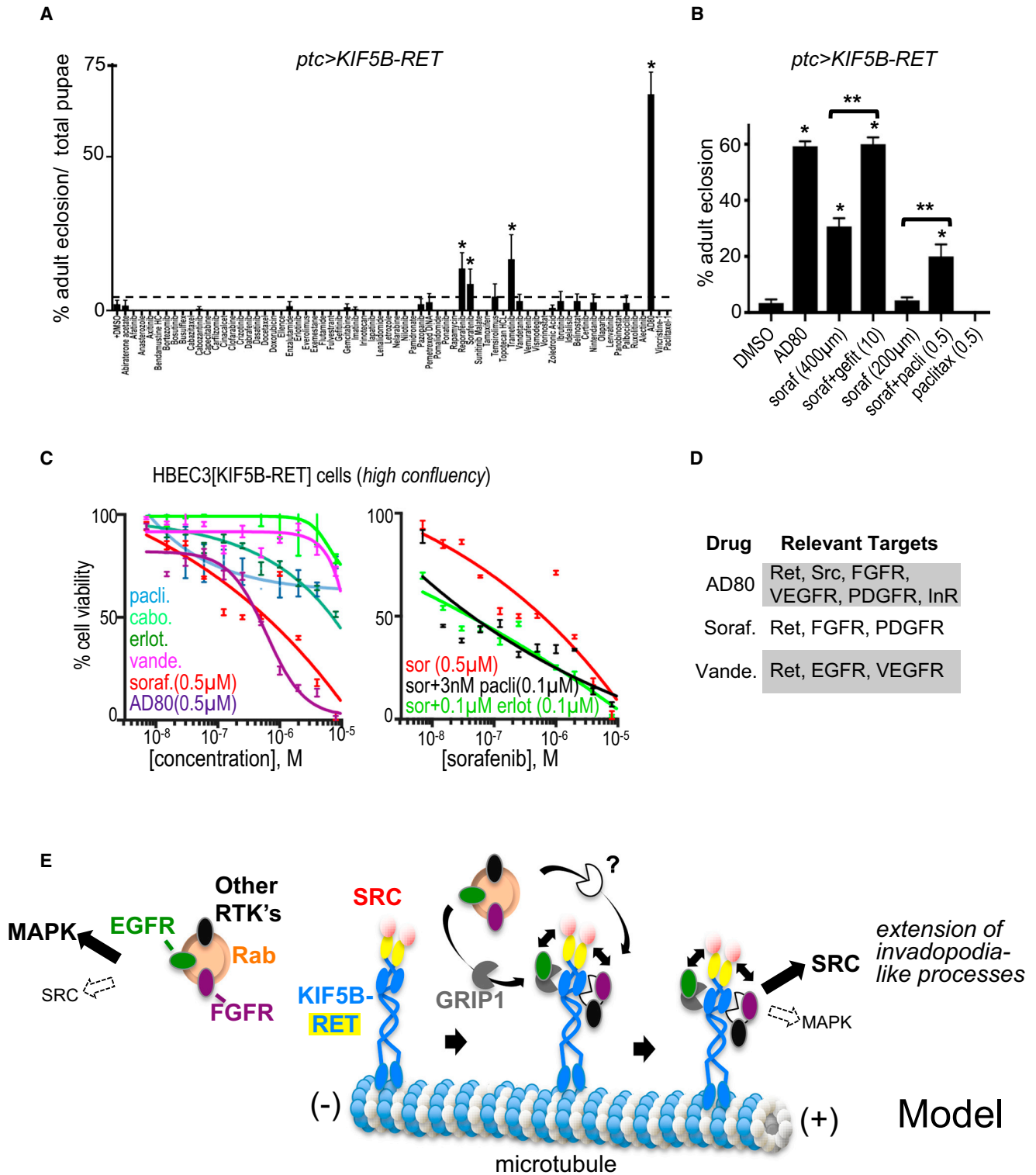


Figure 7. Inhibiting EGFR Signaling Is Optimal for Therapeutics Targeting the KIF5B-RET Network

(A) Screening a panel of 66 FDA-approved and investigational drugs (see list in Figure S6) in a *ptc>KIF5B-RET* fly viability assay. Means are shown as column graphs, and SEMs are shown as error bars. The ratio represents the mean of the number of adults to the number of pupae per vial; see [Experimental Procedures](#). Asterisks indicate a significance of $p < 0.05$ for each genotype compared to DMSO control (mean = 2.1%). RET inhibitors regorafenib (13.7%), sorafenib (8.6%), and AD80 (70.3%) and MEK inhibitor trametinib (16.7%) showed ability to improve pupae-to-adult survival.

(legend continued on next page)

were plated with 50%–60% confluency in 100 cm² tissue culture plates in respective media and allowed to grow for 4 or 5 days. Cells were washed with cold 1× PBS and scraped into 1× lysis buffer from the kit, and lysates were extracted. A Bio-Rad protein assay was used to assess the protein concentration of the lysate. An antibody array was incubated with lysates at 0.5 mg/mL total protein concentration, as recommended by the manufacturer, and developed according to manufacturer protocols.

Tissue Culture Studies

Cells were grown in airway epithelial basal media supplemented with a bronchial epithelial growth kit from ATCC. Cells were transfected with lipofectamine or HiPerFect for siRNA experiments, and cell lysis was performed 24 and 48 hr after transfection. For imaging studies, cells were grown to 50% or 100% confluency in Lab-Tek II 8-chamber slides (Fisher), transfected, and grown for a further 24–48 hr in media.

Western Blot of Fly Wing Discs

30 third instar discs of each genotype (*765 > UAS-transgene*) were dissolved in lysis buffer (50 mM Tris, 150 mM NaCl, 1% Triton X-100, 1 mM EDTA) supplemented with a protease inhibitor cocktail (Sigma) and a phosphatase inhibitor cocktail (Sigma). Total protein in each sample was quantitated using a Bio-Rad protein assay. Samples were resolved on Invitrogen NuPAGE gradient SDS-PAGE and transferred by standard protocols. Membranes were stripped with Sigma Restore stripping buffer and reprobed with other antibodies to assess the signal under the same loading conditions.

Western Blot of Cancer Cell Lines

HBEC3 cell lines were grown in 100 cm² well plates in bronchial airway epithelial media (ATCC), each supplemented with penicillin and streptomycin antibiotics. After required growth, cells were washed twice with cold PBS, lysed in radioimmunoprecipitation assay (RIPA) buffer (25 mM Tris [pH 7.6], 150 mM NaCl, 1% NP-40, 0.1% SDS) containing protease and phosphatase inhibitors, and sonicated (Roche). Lysate protein concentration was assessed using a Bio-Rad protein assay. 5 or 10 μg of the total cell lysate were separated by SDS-PAGE, transferred to a polyvinylidene fluoride (PVDF) membrane, and blotted for the indicated proteins using commercial antibodies. Membranes were stripped and probed as described earlier.

Whole-Mount Imaging of Fly Wings

For adult wing vein analysis, wings were dissected and kept in 100% ethanol overnight, mounted on slides in 80% glycerol in PBS solution, and imaged by regular light microscopy using a Leica DM5500 Q microscope.

SUPPLEMENTAL INFORMATION

Supplemental Information includes seven figures and can be found with this article online at <http://dx.doi.org/10.1016/j.celrep.2017.08.037>.

AUTHOR CONTRIBUTIONS

T.K.D. and R.L.C. conceived and designed the project. T.K.D. performed all experiments. T.K.D. and R.L.C. acquired research funds. T.K.D. and R.L.C. wrote the manuscript.

ACKNOWLEDGMENTS

We thank members of the Cagan laboratory, including Vanessa Barcessat, for technical assistance and helpful discussions. We thank the Bloomington *Drosophila* Stock Center for *Drosophila* reagents. Microscopy was performed partly at the Microscopy Shared Resource Facility at the Icahn School of Medicine at Mount Sinai. This research was supported by NIH grants R01-CA170495 and R01-CA109730; Department of Defense grant W81XWH-15-1-0111; and American Cancer Society grants 120886-PFM-11-137-01-DDC (T.K.D.) and 120616-RSGM-11-018-01-CDD (R.L.C.).

Received: April 14, 2017

Revised: June 30, 2017

Accepted: August 8, 2017

Published: September 5, 2017

REFERENCES

- Apfel, B., Blair, J.A., Gonzalez, B., Nazif, T.M., Feldman, M.E., Aizenstein, B., Hoffman, R., Williams, R.L., Shokat, K.M., and Knight, Z.A. (2008). Targeted polypharmacology: discovery of dual inhibitors of tyrosine and phosphoinositide kinases. *Nat. Chem. Biol.* 4, 691–699.
- Begley, M.J., Yun, C.-H., Gewinner, C.A., Asara, J.M., Johnson, J.L., Coyle, A.J., Eck, M.J., Apostolou, I., and Cantley, L.C. (2015). EGF-receptor specificity for phosphotyrosine-primed substrates provides signal integration with Src. *Nat. Struct. Mol. Biol.* 22, 983–990.
- Beldjord, C., Desclaux-Arromond, F., Raffin-Sanson, M., Corvol, J.C., De Keyzer, Y., Luton, J.P., Plouin, P.F., and Bertagna, X. (1995). The RET protooncogene in sporadic pheochromocytomas: frequent MEN 2-like mutations and new molecular defects. *J. Clin. Endocrinol. Metab.* 80, 2063–2068.
- Boumahdi, S., Driessens, G., Lapouge, G., Rorive, S., Nassar, D., Le Mercier, M., Delatte, B., Caauwe, A., Lenglez, S., Nkusi, E., et al. (2014). SOX2 controls tumour initiation and cancer stem-cell functions in squamous-cell carcinoma. *Nature* 511, 246–250.
- Buszczak, M., Paterno, S., Lighthouse, D., Bachman, J., Planck, J., Owen, S., Skora, A.D., Nystul, T.G., Ohlstein, B., Allen, A., et al. (2007). The Carnegie protein trap library: a versatile tool for *Drosophila* developmental studies. *Genetics* 175, 1505–1531.
- Clark, E.S., Whigham, A.S., Yarbrough, W.G., and Weaver, A.M. (2007). Cortactin is an essential regulator of matrix metalloproteinase secretion and extracellular matrix degradation in invadopodia. *Cancer Res.* 67, 4227–4235.
- Cohen, M.H., Williams, G., Johnson, J.R., Duan, J., Gobburu, J., Rahman, A., Benson, K., Leighton, J., Kim, S.K., Wood, R., et al. (2002). Approval summary for imatinib mesylate capsules in the treatment of chronic myelogenous leukemia. *Clin. Cancer Res.* 8, 935–942.
- Dar, A.C., Das, T.K., Shokat, K.M., and Cagan, R.L. (2012). Chemical genetic discovery of targets and anti-targets for cancer polypharmacology. *Nature* 486, 80–84.
- Das, T.K., Sangodkar, J., Negre, N., Narla, G., and Cagan, R.L. (2013). Sin3a acts through a multi-gene module to regulate invasion in *Drosophila* and human tumors. *Oncogene* 32, 3184–3197.

(B) Drugs and combinations that suppressed pupal lethality in *ptc>KIF5B-RET* flies. 59.2% of AD80-treated flies ($n = 203$) and 30.6% of sorafenib-treated flies (400 μM, $n = 369$) eclosed as adults, versus only 3.4% of DMSO control ($n = 509$). Combined sorafenib and gefitinib treatment ($n = 253$) led to 60% closure as adults. Sorafenib (200 μM, $n = 330$) in combination with paclitaxel (0.5 μM) significantly increased viability ($n = 435$) to 20%.

(C) Effect of various inhibitors on the growth rate of human *HBEC3[KIF5B-RET]* cells. The dose response curve was fitted to the non-linear regression model using PRISM software; IC_{50} is in brackets. Left panel: confluent cells showed weak sensitivity to clinically approved RET inhibitors vandetanib or cabozantinib ($IC_{50} > 10$ μM) but were sensitive to both sorafenib and AD80 ($IC_{50} \sim 0.5$ μM). EGFR inhibitor erlotinib showed an intermediate effect ($IC_{50} \sim 10$ μM). Right panel: the combination of sorafenib and erlotinib or sorafenib and paclitaxel potently inhibited ($IC_{50} \sim 0.1$ μM) growth of *HBEC3[KIF5B-RET]* cells. Doses of paclitaxel (3 nM) and erlotinib (0.1 μM) used in the combinations had little effect on growth of *HBEC3[KIF5B-RET]* cells by themselves (left panel).

(D) Summary table of the KIF5B network of relevant targets for the drugs AD80, sorafenib, and vandetanib.

(E) Model: KIF5B-RET fusion protein recruits pEGFR, pGFR, and other RTKs from RAB vesicles via GRIP1 and other cofactors. pSRC activated by RET kinase domain cooperates with the recruited RTKs for optimal signaling. EGFR signaling in lung cells is MAPK dominant (pEGFR[Y1068]), but active SRC switches EGFR signaling to a SRC dominant (pEGFR[Y845]) form.

- Drlon, A., Rekhman, N., Arcila, M., Wang, L., Ni, A., Albano, M., Van Voorthuyzen, M., Somwar, R., Smith, R.S., Montecalvo, J., et al. (2016). Cabozantinib in patients with advanced RET-rearranged non-small-cell lung cancer: an open-label, single-centre, phase 2, single-arm trial. *Lancet Oncol.* **17**, 1653–1660.
- Forde, P.M., and Rudin, C.M. (2012). Crizotinib in the treatment of non-small-cell lung cancer. *Expert Opin. Pharmacother.* **13**, 1195–1201.
- Galetta, D., Rossi, A., Pisconti, S., and Colucci, G. (2012). The emerging role of ALK inhibitors in the treatment of advanced non-small cell lung cancer. *Expert Opin. Ther. Targets* **16** (Suppl 2), S45–S54.
- Gautschi, O., Milia, J., Filleron, T., Wolf, J., Carbone, D.P., Owen, D., Camidge, R., Narayanan, V., Doebele, R.C., Besse, B., et al. (2017). Targeting RET in patients with RET-rearranged lung cancers: results from the global, multicenter RET registry. *J. Clin. Oncol.* **35**, 1403–1410.
- Gibson, N.J., Tolbert, L.P., and Oland, L.A. (2012). Activation of glial FGFRs is essential in glial migration, proliferation, and survival and in glia-neuron signaling during olfactory system development. *PLoS ONE* **7**, e33828.
- Groth, A.C., Fish, M., Nusse, R., and Calos, M.P. (2004). Construction of transgenic *Drosophila* by using the site-specific integrase from phage ϕ C31. *Genetics* **166**, 1775–1782.
- Hirokawa, N., Noda, Y., Tanaka, Y., and Niwa, S. (2009). Kinesin superfamily motor proteins and intracellular transport. *Nat. Rev. Mol. Cell Biol.* **10**, 682–696.
- Hoshino, D., Kirkbride, K.C., Costello, K., Clark, E.S., Sinha, S., Grega-Larson, N., Tyska, M.J., and Weaver, A.M. (2013). Exosome secretion is enhanced by invadopodia and drives invasive behavior. *Cell Rep.* **5**, 1159–1168.
- Jemal, A., Center, M.M., DeSantis, C., and Ward, E.M. (2010). Global patterns of cancer incidence and mortality rates and trends. *Cancer Epidemiol. Biomarkers Prev.* **19**, 1893–1907.
- Ju, Y.S., Lee, W.C., Shin, J.Y., Lee, S., Bleazard, T., Won, J.K., Kim, Y.T., Kim, J.I., Kang, J.H., and Seo, J.S. (2012). A transforming KIF5B and RET gene fusion in lung adenocarcinoma revealed from whole-genome and transcriptome sequencing. *Genome Res.* **22**, 436–445.
- Karim, F.D., and Rubin, G.M. (1998). Ectopic expression of activated Ras1 induces hyperplastic growth and increased cell death in *Drosophila* imaginal tissues. *Development* **125**, 1–9.
- Kohno, T., Ichikawa, H., Totoki, Y., Yasuda, K., Hiramoto, M., Nammo, T., Sakamoto, H., Tsuta, K., Furuta, K., Shimada, Y., et al. (2012). KIF5B-RET fusions in lung adenocarcinoma. *Nat. Med.* **18**, 375–377.
- Lam, E.T., Ringel, M.D., Kloos, R.T., Prior, T.W., Knopp, M.V., Liang, J., Sammet, S., Hall, N.C., Wakely, P.E., Jr., Vasko, V.V., et al. (2010). Phase II clinical trial of sorafenib in metastatic medullary thyroid cancer. *J. Clin. Oncol.* **28**, 2323–2330.
- Levinson, S., and Cagan, R.L. (2016). *Drosophila* cancer models identify functional differences between Ret fusions. *Cell Rep.* **16**, 3052–3061.
- Lin, C., Wang, S., Xie, W., Zheng, R., Gan, Y., and Chang, J. (2016). Apatinib inhibits cellular invasion and migration by fusion kinase KIF5B-RET via suppressing RET/Src signaling pathway. *Oncotarget* **7**, 59236–59244.
- Lipson, D., Capelletti, M., Yelensky, R., Otto, G., Parker, A., Jarosz, M., Curran, J.A., Balasubramanian, S., Bloom, T., Brennan, K.W., et al. (2012). Identification of new ALK and RET gene fusions from colorectal and lung cancer biopsies. *Nat. Med.* **18**, 382–384.
- Liu, Z., Falola, J., Zhu, X., Gu, Y., Kim, L.T., Sarosi, G.A., Anthony, T., and Nwariaku, F.E. (2004). Antiproliferative effects of Src inhibition on medullary thyroid cancer. *J. Clin. Endocrinol. Metab.* **89**, 3503–3509.
- Mader, C.C., Oser, M., Magalhaes, M.A.O., Bravo-Cordero, J.J., Condeelis, J., Koleske, A.J., and Gil-Henn, H. (2011). An EGFR-Src-Arg-cortactin pathway mediates functional maturation of invadopodia and breast cancer cell invasion. *Cancer Res.* **71**, 1730–1741.
- Martín-Blanco, E., Roch, F., Noll, E., Baonza, A., Duffy, J.B., and Perrimon, N. (1999). A temporal switch in DER signaling controls the specification and differentiation of veins and interveins in the *Drosophila* wing. *Development* **126**, 5739–5747.
- McCoach, C.E., and Doebele, R.C. (2014). The minority report: targeting the rare oncogenes in NSCLC. *Curr. Treat. Options Oncol.* **15**, 644–657.
- Mertens, F., Johansson, B., Fioretos, T., and Mitelman, F. (2015). The emerging complexity of gene fusions in cancer. *Nat. Rev. Cancer* **15**, 371–381.
- Pao, W., Miller, V., Zakowski, M., Doherty, J., Politi, K., Sarkaria, I., Singh, B., Heelan, R., Rusch, V., Fulton, L., et al. (2004). EGF receptor gene mutations are common in lung cancers from “never smokers” and are associated with sensitivity of tumors to gefitinib and erlotinib. *Proc. Natl. Acad. Sci. USA* **101**, 13306–13311.
- Plaza-Menacho, I., Barnouin, K., Goodman, K., Martínez-Torres, R.J., Borg, A., Murray-Rust, J., Mouilleron, S., Knowles, P., and McDonald, N.Q. (2014). Oncogenic RET kinase domain mutations perturb the autophosphorylation trajectory by enhancing substrate presentation in trans. *Mol. Cell* **53**, 738–751.
- Read, R.D., Goodfellow, P.J., Mardis, E.R., Novak, N., Armstrong, J.R., and Cagan, R.L. (2005). A *Drosophila* model of multiple endocrine neoplasia type 2. *Genetics* **171**, 1057–1081.
- Rothenberg, S.M., Concannon, K., Cullen, S., Boulay, G., Turke, A.B., Faber, A.C., Lockerman, E.L., Rivera, M.N., Engelman, J.A., Maheswaran, S., and Haber, D.A. (2015). Inhibition of mutant EGFR in lung cancer cells triggers SOX2-FOXO6-dependent survival pathways. *eLife* **4**, 1–25.
- Sarfaty, M., Moore, A., Neiman, V., Dudnik, E., Ilouze, M., Gottfried, M., Katznelson, R., Nechushtan, H., Sorotsky, H.G., Paz, K., et al. (2017). RET fusion lung carcinoma: response to therapy and clinical features in a case series of 14 patients. *Clin. Lung Cancer* **18**, e223–e232.
- Sato, M., Vaughan, M.B., Girard, L., Peyton, M., Lee, W., Shames, D.S., Ramirez, R.D., Sunaga, N., Gazdar, A.F., Shay, J.W., and Minna, J.D. (2006). Multiple oncogenic changes (K-RAS(V12), p53 knockdown, mutant EGFRs, p16 bypass, telomerase) are not sufficient to confer a full malignant phenotype on human bronchial epithelial cells. *Cancer Res.* **66**, 2116–2128.
- Setou, M., Seog, D.-H., Tanaka, Y., Kanai, Y., Takei, Y., Kawagishi, M., and Hirokawa, N. (2002). Glutamate-receptor-interacting protein GRIP1 directly steers kinesin to dendrites. *Nature* **417**, 83–87.
- Siegle, J.M., Basin, A., Sastre-Perona, A., Yonekubo, Y., Brown, J., Sennett, R., Rendl, M., Tsirigos, A., Carucci, J.A., and Schober, M. (2014). SOX2 is a cancer-specific regulator of tumour initiating potential in cutaneous squamous cell carcinoma. *Nat. Commun.* **5**, 4511.
- Takeuchi, K., Soda, M., Togashi, Y., Suzuki, R., Sakata, S., Hatano, S., Asaka, R., Hamaoka, W., Ninomiya, H., Uehara, H., et al. (2012). RET, ROS1 and ALK fusions in lung cancer. *Nat. Med.* **18**, 378–381.
- Vaishnavi, A., Schubert, L., Rix, U., Marek, L.A., Le, A.T., Keysar, S.B., Glogowska, M.J., Smith, M.A., Kako, S., Sumi, N.J., et al. (2017). EGFR mediates responses to small-molecule drugs targeting oncogenic fusion kinases. *Cancer Res.* **77**, 3551–3563.
- Vidal, M., Larson, D.E., and Cagan, R.L. (2006). Csk-deficient boundary cells are eliminated from normal *Drosophila* epithelia by exclusion, migration, and apoptosis. *Dev. Cell* **10**, 33–44.
- Wright, T.I., and Petersen, J.E. (2007). Treatment of recurrent dermatofibrosarcoma protuberans with imatinib mesylate, followed by Mohs micrographic surgery. *Dermatol. Surg.* **33**, 741–744.
- Yoh, K., Seto, T., Satouchi, M., Nishio, M., Yamamoto, N., Murakami, H., Nogami, N., Matsumoto, S., Kohno, T., Tsuta, K., et al. (2017). Vandetanib in patients with previously treated RET-rearranged advanced non-small-cell lung cancer (LURET): an open-label, multicentre phase 2 trial. *Lancet Respir. Med.* **5**, 42–50.
- Yokomaku, D., Jourdi, H., Kakita, A., Nagano, T., Takahashi, H., Takei, N., and Nawa, H. (2005). ErbB1 receptor ligands attenuate the expression of synaptic scaffolding proteins, GRIP1 and SAP97, in developing neocortex. *Neuroscience* **136**, 1037–1047.